



Image Warping Using Radial Basis Functions

Journal:	<i>Journal of Applied Statistics</i>
Manuscript ID:	CJAS-2013-0101.R1
Manuscript Type:	Original Article
Date Submitted by the Author:	n/a
Complete List of Authors:	Chen, Ting-Li; Academia Sinica, Institute of Statistical Sciences Geman, Stuart; Brown University, Division of Applied Mathematics
Keywords:	Thin plate spline, image warping, image morphing, data interpolation, optimization

SCHOLARONE™
Manuscripts

Journal of Applied Statistics

Vol. 00, No. 00, February 2013, 1–14

RESEARCH ARTICLE

Image Warping Using Radial Basis Functions

Ting-Li Chen^{a*} and Stuart Geman^b^a*Institute of Statistical Science, Academia Sinica, Taipei 11529, Taiwan;*^b*Division of Applied Mathematics, Brown University, RI 02912, USA*

(2013)

Image warping is the process of deforming an image through a transformation of its domain, which is typically a subset of R^2 . Given the destination of a collection of points, the problem becomes one of finding a suitable smooth interpolation for the destinations of the remaining points of the domain. A common solution is to use the thin plate spline. We find that the thin plate spline often introduces unintended distortions of image structures. In this paper, we will analyze interpolation by thin plate spline, experiment with other radial basis functions, and suggest two alternative functions that provide better results.

1. Introduction

Image warping is sometimes referred to as “rubber sheet transformation”: an image printed on a rubber sheet is distorted geometrically as the rubber sheet is stretched to reposition previously chosen control points. Image warping has applications in various image processing and image analysis tasks, such as image registration, image morphing, object identification and recognition, and computer animation.

To warp one image to another, we might first compute the offsets for a collection of control points that are easily matched. The problem is then to:

Find a “good” mapping f from R^2 to R^2 , under the constraint that $f(p_i) = p'_i$ for $i = 1, \dots, n$, where p_i and $p'_i \in R^2$.

Since the mapping $f = (f_x, f_y)$ can be constructed separately in each dimension, the problem reduces to:

Find a “good” mapping f from R^2 to R , under the constraint that $f(p_i) = h_i$ for $i = 1, \dots, n$, where $p_i \in R^2$ and $h_i \in R$.

The offset h_i can be viewed as the height of a surface at the location p_i , and the mapping f can then be viewed as a surface passing through a given set of points in 3-D space. This problem is called the “scattered data interpolation problem,” and various approaches for constructing a smooth interpolation have been devised. Good reviews can be found in [2, 18, 29, 40].

One of the first ideas on scattered data interpolation is based on an inverse-distance weighting of data known as Shepard’s method [39]. Similar ideas were applied earlier in [7] and [9]. The basic idea of Shepard’s method is to interpolate by the weighted average of the data, with weights proportional to inverse distance.

*Corresponding author. Email: tlchen@stat.sinica.edu.tw

Explicitly, the interpolating function is

$$f(x, y) = \frac{\sum_{k=1}^n \frac{f_k}{[d_k(x, y)]^\mu}}{\sum_{k=1}^n \frac{1}{[d_k(x, y)]^\mu}},$$

where $d_k(x, y) = \sqrt{(x - x_k)^2 + (y - y_k)^2}$, f_k is the data value at (x_k, y_k) , and μ is a constant popularly chosen as two. This method, however, introduces serious artifacts such as “cusps”, “flat spots”, “corners”, and undue influence of points which are far away [19]. Later works have addressed these shortcomings and achieved considerable improvements; see [17, 35, 37].

Another classic approach is through triangulation. The first step is to partition an image into disjoint triangles by connecting control points. Then each triangle is interpolated locally. An “optimal” triangulation is very important to this approach. Delaunay triangulation [10], which maximizes the minimum inner angle of triangles, is a popular triangulation method that avoids triangles with small angles. Reviews on triangulation methods can be found in [26, 38]. After the triangulation step, various methods can be applied to each triangle locally. Piecewise linear interpolation, for example, is continuous but not smooth across triangle boundaries. To address the issue of smoothness, higher-ordered bivariate polynomials have been suggested [1, 21, 33, 34] based on the Clough-Tocher method [6]. Reviews on triangular interpolants can be found in [30, 32].

Another popular approach to scattered data interpolation is to construct the interpolation function f as a linear combination of basis functions g_k . Each basis function is radially symmetric to a data point (“radial basis function”). The formula is:

$$f(x, y) = \sum_{k=1}^N a_k g_k(d_k(x, y)),$$

where $d_k(x, y) = \sqrt{(x - x_k)^2 + (y - y_k)^2}$. We will focus on the typical case in which g_k depends on k only through d_k , and hereafter write g instead of g_k . This method is first mentioned in Hardy [23]. The basis functions used by Hardy were the multiquadric functions $g(d_k) = \sqrt{d_k^2 + c^2}$; see [24]. The approach was then extended by adding a polynomial of degree m :

$$f(x, y) = \sum_{k=1}^N a_k g(d_k(x, y)) + \sum_{k=1}^M b_k p_k(x, y), \quad (1)$$

where $\{p_k\}$ is the set of polynomials of the form $x^i y^j$, $0 \leq i + j \leq m$ and $M = (m + 2)(m + 1)/2$, and where the following constraints determine the $N + M$ coefficients:

$$\sum_{k=1}^N a_k g(d_k(x_i, y_i)) + \sum_{k=1}^M b_k p_k(x_i, y_i) = f(x_i, y_i) \quad i = 1, \dots, N$$

$$\sum_{i=1}^N a_k p_k(x_i, y_i) = 0 \quad k = 1, \dots, M.$$

The last M equations guarantee polynomial precision. Concerning g , linear, cu-

1 bic, Gaussian, and shifted logarithms have also been used, in addition to Hardy's
2 multiquadric functions.

3 The thin plate spline (TPS) corresponds to the radial basis function $r^2 \log r^2$,
4 and was derived by Duchon [11] through a variational formulation that minimizes
5 the bending energy of a thin plate. The idea can be found earlier, described as a
6 surface spline, in Harder and Desmarais [22]. This method has become popular in
7 image processing after being introduced to the field by Bookstein [3, 4]. Reviews
8 on image warping in general can be found in [20, 36, 41, 42].

9 Instead of moving control points, another approach of warping is by moving
10 control line segments [27, 28, 31]. In this paper we focus on image warping using
11 radial basis functions, which would be a simple modification of the popular TPS.
12 Section 2 starts with an introduction to the thin plate spline. In Section 3 we
13 present examples that demonstrate situations in which TPS produces poor results.
14 In Section 4 we experiment with other radial basis functions applied to these same
15 examples, as well as to an example with real data in Section 5. Based on our
16 experiments we recommend two radial basis functions that often produce the best
17 warping results.
18
19
20
21
22
23

24 2. Thin Plate Spline

25 Imagine that the interpolating surface is a thin sheet of metal. The thin sheet is
26 initially flat, and then bent to pass through a set of data points. The "best" surface
27 is the one with the least bend. Formally, we seek the surface that minimizes the
28 bending energy:
29

$$30 E_f = \int \int_{R^2} (f_{xx}^2 + 2f_{xy}^2 + f_{yy}^2) dx dy.$$

31
32
33
34
35 Duchon [11] showed that the f with minimal bending energy has the form:
36

$$37 f(x, y) = a_1 + a_x x + a_y y + \sum_{i=1}^n w_i g(|p_i - (x, y)|),$$

38
39
40
41
42
43 where $g(r) = r^2 \log r^2$, $p_i = (x_i, y_i)$, and $|p_i - (x, y)|$ is the Euclidean distance
44 from p_i to (x, y) . There are $n + 3$ unknown variables $(a_1, a_x, a_y, w_1, \dots, w_n)$ to
45 be determined from the n equations $f(x_i, y_i) = h_i$, for $i = 1, \dots, n$. Since E_f is
46 finite, the second derivatives of f have to be square-integrable, and this leads to
47 the following three additional constraints:
48
49

$$50 \sum_{i=1}^n w_i = 0,$$

$$51 \sum_{i=1}^n w_i x_i = 0,$$

$$52 \sum_{i=1}^n w_i y_i = 0.$$

4

Taylor & Francis and I.T. Consultant

Let

$$K = [g(|(x_i, y_i) - (x_j, y_j)|)]_{n \times n},$$

$$P = \begin{bmatrix} 1 & x_1 & y_1 \\ 1 & x_2 & y_2 \\ \vdots & \vdots & \vdots \\ 1 & x_n & y_n \end{bmatrix}_{n \times 3},$$

$$L = \begin{bmatrix} K & P \\ P^T & O \end{bmatrix}_{(n+3) \times (n+3)}, \quad (2)$$

$$H = (h_1, \dots, h_n, 0, 0, 0)^T,$$

$$W = (w_1, \dots, w_n, a_1, a_x, a_y)^T,$$

where T is the matrix transpose, and O is the 3×3 matrix of zeros. Then

$$L \times W = H$$

and

$$W = L^{-1} \times H.$$

Note that L is singular if the rank of P is smaller than 3, meaning that all data points are on the same straight line.

Duchon [11] in fact studies a more general case. Let $(x_i, h_i)_{i=1, \dots, n}$ be the scattered data, where $x_i = (x_i(1), \dots, x_i(d)) \in R^d$ and $h_i \in R$. Now the task is to minimize

$$\int_{R^d} \sum_{|v|=m} (D^v f)^2 dx,$$

where $v = (v_1, v_2, \dots, v_d)$, $|v| = \sum_{i=1}^d v_i$, and $D^v = \frac{\partial^{|v|}}{\partial x(1)^{v_1} \dots \partial x(d)^{v_d}}$. For $2m > d$, the solution has the form:

$$f(x) = p_m(x) + \sum_{i=1}^n w_i g(|x - x_i|),$$

where p_m is a polynomial function of degree less than m , and

$$g(r) = \begin{cases} r^{2m-d} \log r, & \text{if } d \text{ is even} \\ r^{2m-d}, & \text{if } d \text{ is odd.} \end{cases} \quad (3)$$

The thin plate spline is the special case with $m = d = 2$, i.e. $g(r) = r^2 \log r = 0.5r^2 \log r^2$. For $m = 2$ and $d = 1$, $g(r) = r^3$, the cubic spline in one dimension. From this point of view, the thin plate spline is seen as a generalization of the cubic spline.

Duchon [12] further generalized the result to minimizing

$$\int_{R^d} |x|^{2s} \sum_{|v|=m} (\widehat{D^v f})^2 dx, \quad 0 < s < 1,$$

where $\hat{\cdot}$ denotes the Fourier transform of the appropriate derivative of f . For $2m + 2s > d$, the corresponding $g(r)$ is

$$g(r) = \begin{cases} r^{2m+2s-d} \log r, & \text{if } 2m + 2s - d \text{ is even} \\ r^{2m+2s-d}, & \text{otherwise.} \end{cases} \quad (4)$$

Additional theoretical developments of radial basis functions can be found in [5], [13] and [14].

Another perspective comes from the equivalence between interpolation with radial basis functions and kriging, as studied in spatial statistics. This perspective provides yet another way to derive or design g , in this case through a presumed spatial covariance structure. The related theories can be found in [8] and [25].

3. Problem with the Thin Plate Spline

The physical interpretation of the TPS algorithm, and the attendant theoretical justification of $g(r) = r^2 \log r^2$, contributes to its popularity in the image processing community. This clear conceptualization, however, does not guarantee good performance on image-processing tasks.

3.1 Example 1

The image to be warped is shown in Figure 1(a). Our goal is to modify the shape of BCD so that the overall shape is a rectangle. We chose eight control points, among which A, B, D, E, F, G, and H were fixed, and C was to be moved, upward, to the midpoint of B and D. Figure 1(b) shows the result of applying the TPS interpolating warp.

While points on \overline{BC} and \overline{CD} were moved upward, TPS, by minimizing sharp bends (large second derivatives) in the displacement field, also moved points on \overline{AB} and \overline{DE} , and on the more distant \overline{FG} and \overline{GH} , downward. These edges, straight in the original image (Figure 1(a)), are now noticeably curved (Figure 1(b)).

3.2 Example 2

These undesirable, global, properties of TBS interpolation can be further illustrated and explored in the simple setting of $f : R^2 \rightarrow R^1$. The original function is a flat surface with $z = f(x, y) = 0$. We chose the twenty-five control points $(i, j, 0)$, $i, j \in \{-2, -1, 0, 1, 2\}$. The goal is to move $(0,0,0)$ up to $(0,0,1)$, while not moving the remaining twenty-four points.

The original function and the control points are shown in Figure 2(a), and the TPS interpolating surface in Figure 2(b). We use gray-level intensities to represent height and black dots to indicate the locations of the twenty-five control points.

Comparing Figure 2(a) to Figure 2(b), we observe that the region outside of the control points is lighter in (b), and the regions between some of the control points is darker in (b). These effects can also be seen in Figure 2(c), a three-dimensional view. In Figure 2(d) we display the intersection of the surface with $y=0$, clearly showing the surface to be below $z=0$ on $(-2, -1)$ and $(1, 2)$, between control points, and above $z=0$ outside $[-2, 2]$, where there are no control points. Evidently, there are artifacts both near to and far removed from the control points.

4. Other Radial Basis Functions

As there is abundant literature in scattered data interpolation, Franke [16] examined and compared many methods on the basis of the accuracy and visual impression of their reconstructed surfaces. The conclusion was that TPS and Hardy's multiquadric methods [23] generally achieve the best performance.

In this section, we evaluate the performance of a variety of scattered data interpolation methods, with the goal of identifying the best methods specifically for image warping. We use the two examples from the previous section as a basis for comparison.

4.1 Multiquadric: $g(r) = \sqrt{r^2 + k}$

The multiquadric function proposed by Hardy [23] was the first radial basis function applied to interpolation, and was shown by Franke [16] to produce good results. Hardy proposed to use $k = 0.815m$, where m is the mean squared distance between points. Referring to example 2 from Section 3, where $m = 8$, Hardy's proposal would be to take $k = 0.815 \times 8 = 6.52$. We experimented with $k=0, 6.52, 30$ and 100. Figure 3 shows the results. In a manner similar to the TPS solution, the intersection of $y = 0$ with the interpolating surface is below zero on $(-2, 1)$ and $(1,2)$. But the result improves with decreasing k . Franke, using the smoothness of a curve or surface as an evaluation criterion, concluded that the $k = 0$ solution was undesirable due to high curvatures at ± 1 . However, for the purpose of image warping, the excellent localization of the $k = 0$ perturbation to the interval $(-1, 1)$ is an important virtue.

We applied $g(r) = \sqrt{r^2 + k}$ with $k = 0$ and $k = 0.815m = 6.52$ to the first example of Section 3. The results, as seen in Figure 4, are again excellent when $k = 0$ (left-hand panel); the suggested parameter value, $k = 0.815m$ (right-hand panel), is obviously inferior. It is interesting to note that $g(r) = r$ can be derived from Duchon's generalization of "bending energy" to variational problems in the Fourier domain – see equation 4 with $m = 1, d = 2$, and $s = 0.5$.

4.2 Inverse Multiquadric: $g(r) = \frac{1}{\sqrt{r^2 + k}}$

Here we evaluate a second proposal by Hardy: the so-called inverse multiquadric basis function, $g(r) = \frac{1}{\sqrt{r^2 + k}}$. Following the development in 4.1, we applied the inverse multiquadric with a range of values of k ($k = 1, 10, 100$ and 1000) to the second example of Section 3. The results are shown in Figure 5. When $k=1$ and 10, the curves are entirely above zero, whereas when $k=100$ and 1000, the curves are similar to those of the TPS and the multiquadric function. In general $\sqrt{r^2 + 100}$ and $\frac{1}{\sqrt{r^2 + 100}}$ produce similar results, and we selected $k = 100$ ($g(r) = \frac{1}{\sqrt{r^2 + 100}}$) as the best of the inverse multiquadric solutions that we tested. But the application to example 1 of Section 3 does not produce the desired straight line along the \overline{BD} segment, as can be seen in Figure 6.

4.3 Shifted Thin Plate Spline

Dyn et al. [15] proposed a variation on the thin plate spline:

$$g(r) = (r^2 + k) \log(r^2 + k).$$

Setting $k = 0$ recovers the original TPS. We applied the “shifted TPS” with $k=0$, 1, 10 and 100 to example 2 of Section 3. As seen in Figure 7, increasing in k from 0 serves to enhance, rather than diminish, the influence of local changes. The original TPS appears to be the better choice for image warping.

4.4 $g(r) = r^k$

Our earlier experiments with the multiquadric function $g(r) = \sqrt{r^2 + k}$ (cf. Figures 3 and 4) produced good results in the special case $k = 0$, i.e. using the simple radial basis function $g(r) = r$. Here we generalized to $g(r) = r^k$ and experimented with $k = 0.5, 1.5, 2.5$ and 3. (As shown in the Appendix, the matrix L in (2) is always singular for $k = 2$ and $n \geq 4$; hence no experiments were performed with $k = 2$.)

The previous experiments suggested that TPS ($r^2 \log r^2$) tends to over-smooth, and that this is largely corrected by using the function r instead, which has a less global influence. Referring to Figure 8 and example 2 of Section 3, it is therefore not surprising that the curves from the more global basis functions $r^{2.5}$ and r^3 behave poorly, while those from $r^{0.5}$ and $r^{1.5}$ behave similarly to the curves from the basis function r . We applied $g(r) = r^{0.5}$ and $r^{1.5}$ to example 1 – see Figure 9. The image warped by $r^{0.5}$ contains an unacceptable discontinuity at point C (exaggerated for visualization), and the result using $r^{1.5}$, although an improvement over TPS, is still inferior to the $g(r) = r$ result.

4.5 $g(r) = r \log r$

With the goal of localizing the influences of TPS, we also considered $g(r) = r \log r$. As seen in Figures 10 and 11, the results are good and generally in line with those from the simple radial basis function $g(r) = r$.

4.6 *Gaussian*

Using example 2, we experimented with the popular Gaussian radial basis function $g(r) = e^{-r^2/k^2}$, for a range of values of k including $k = 1, 3, 10$, and 30 (see Figure 12). The best performance was at about $k = 10$ ($g(r) = e^{-r^2/100}$), but the result of an application to example 1 (Figure 13) includes a discontinuity at C and is clearly inferior to $g(r) = r$ (Figure 4(a)).

4.7 *Other Basis Functions*

We tested many other radial basis functions. In general, the best performance on the chosen examples (examples 1 and 2 in sections 3.1 and 3.2) was achieved by functions that approximate the simple radial basis function $g(r) = r$ tested in 4.1. Notice that for any constants α and β , $g(r) = \alpha + \beta r$ gives the identical interpolation as $g(r) = r$, as can be seen from a glance at equation 1 and the ensuing equations for the coefficients $\{a_k\}_{k=1:N}$ and $\{b_k\}_{k=1:M}$. Therefore, it is not surprising that performance from each of $g(r) = 1/(r + k)$, $g(r) = \log(r + k)$, and $g(r) = e^{-r/k}$,

for large values of k , was essentially identical to the performance of $g(r) = r$:

$$\frac{\frac{1}{r+k}}{\frac{1}{k} - \frac{1}{k^2}r} \xrightarrow{k \rightarrow \infty} 1 \quad (\alpha = \frac{1}{k}, \beta = -\frac{1}{k^2})$$

$$\frac{\log(r+k)}{\log k + \frac{1}{k}r} \xrightarrow{k \rightarrow \infty} 1 \quad (\alpha = \log k, \beta = \frac{1}{k})$$

$$\frac{e^{-r/k}}{1 - \frac{1}{k}r} \xrightarrow{k \rightarrow \infty} 1 \quad (\alpha = 1, \beta = -\frac{1}{k})$$

4.8 Summary

Our experimental results favor the radial basis functions $g(r) = r$ and $g(r) = r \log r$, and any other functions that closely approximate a linear function of either of these, such as $e^{-r/k}$ for large k . In the next section we will compare the performance of TPS ($r^2 \log r^2$), r , and $r \log r$ on a particularly difficult image-warping task.

5. A Challenging Interpolation Problem

The task is to move selected points at the tips of the fingers of a hand with minimum distortion to the hand and surrounding image. Figure 14(a) shows the image of a hand resting on a textured piece of clothing. Figure 14(b) is identical, except for the addition of twelve control points marked with the symbol *. In each of five experiments, we selected one of the five fingers and computed interpolations that moved the apical control point in one direction or the other, while holding the remaining eleven control points fixed. By examining the hand as a whole, as well as the background texture at points distant to the perturbation, we can quickly assess the strengths and weaknesses of a particular solution. We tested the same three radial basis functions in each experiment, $g(r) = r^2 \log r^2$ (TPS), $g(r) = r$, and $g(r) = r \log r$.

In general, the radial basis functions $g(r) = r$ and $g(r) = r \log r$ performed quite similarly, producing slightly less distortion of both the hand and the background, especially at distant locations. For example, Figure 15 shows the interpolations following movement of the fifth (smallest) finger. As a measure of long-range distortions, Table 1 lists the movements of each of the four corners of the background, relative to its original position (the latter indicated by the black rectangles in Figure 15). Both the total movement of the four corners and the maximum movement among the four corners are also included, for each of the three radial basis functions tested.

Both the visual (Figure 15) and quantitative (Table 1) results are consistent with the relative performances of the three approaches on the artificial examples from Section 3, where it was already observed that TPS produces more local artifact and more distortion at distant locations.

6. Discussion and Conclusion

In this paper, we aimed to identify the best radial basis functions for image warping. The thin plate spline, with radial basis function $g(r) = r^2 \log r^2$, is the most popular method in the image processing community. However, our experiments revealed multiple artifacts. When examining other radial basis functions, we found that

1 results using $g(r) = r$ and $g(r) = r \log r$ were significantly less distorted. We noted
2 that many other basis functions, including $\exp(-r/k)$ (exponential), $\log(r+k)$
3 (shifted logarithm), and $1/(r+k)$ (shifted inverse) produce results similar to $g(r) =$
4 r for large values of k .

5
6 In general, TPS produces long-range effects, leading to distortions at locations
7 distant to the interest points. This can be very difficult to correct in certain applica-
8 tions. For example, in the de-warping of old movies, where the original elements are
9 often found to have undergone local distortions, interest points in and around the
10 warpings are tracked and automatically or manually re-located, with the remaining
11 image locations determined by scattered data interpolation. Good anchor points in
12 the background, which may be initially undistorted, can be hard to find and hard
13 to track, making these areas particularly vulnerable to interpolation artifacts.
14
15

16 17 Acknowledgements

18
19 T.-L. C. is supported by the National Science Council, Taiwan, Grant Nos. NSC
20 98-2118-M-001-024-. S.G. gratefully acknowledge the hospitality and support of the
21 Academia Sinica Mathematics Department, Taipei, Taiwan, and financial support
22 from the Office of Naval Research under contract N000141010933, the National Sci-
23 ence Foundation under grant DMS-1007593, and the Defense Advanced Research
24 Projects Agency under contract FA8650-11-1-7151.
25
26

27 28 29 References

- 30
31 [1] H. Akima, *A Method of Bivariate Interpolation and Smooth Surface Fitting*
32 *for Irregularly Distributed Data Points*, ACM Trans. Math. Software 4 (1978),
33 pp. 148-159.
34 [2] I. Amidror, *Scattered Data Interpolation Methods for Electronic Imaging Sys-*
35 *tems: A Survey*, J. Electronic Imaging 2 (2002), pp. 157-176.
36 [3] F.L. Bookstein, *Principal Warps: Thin-Plate Splines and Decomposition of*
37 *Deformations*, IEEE Trans. Pattern Analysis and Machine Intelligence 11
38 (1989), pp. 567-585.
39 [4] F.L. Bookstein, *Morphometric Tools for Landmark Data: Geometry and Biol-*
40 *ogy*, Cambridge Univ. Press, 1991.
41 [5] M. D. Buhmann, *Radial Basis Functions: Theory and Implementations*, Cam-
42 bridge, U.K.: Cambridge Univ. Press, 2003.
43 [6] R.W. Clough and J.L. Tocher, *Finite Element Stiffness Matrices for Analysis*
44 *of Plates in Bending*, Proc. Conf. on Matrix Methods in Structural Mechanics
45 (1965), pp. 515-545.
46 [7] I. Crain and K. Bhattacharyya, *Treatment of Nonequispaced Two-Dimensional*
47 *Data with a Digital Computer*, Geoexploration 5 (1967), pp. 173-194.
48 [8] N. A. Cressie, *Statistics for spatial data, Revised edition*, John Wiley and Sons,
49 New York, New York, USA, 1993.
50 [9] G.P. Cressman, *An Operational Objective Analysis System*, Mon. Wea. Rev.
51 87 (1959), pp. 367-384.
52 [10] B. Delaunay, *Sur la sphère vide*, Bull. Acad. Science USSR VII: Class. Sci.
53 Mat. Nat (1934), pp. 793-800.
54 [11] J. Duchon, *Interpolation des fonctions de deux variables suivant le principe de*
55 *la flexion des plaques minces*, Analyse Numeriques 10 (1976), pp. 5-12.
56 [12] J. Duchon, *Splines minimizing rotation-invariant semi-norms in Sobolev*
57
58
59
60

- spaces, in *Multivariate Approximation Theory*, W. Schempp and K. Zeller, eds., Birkhäuser, Basel, 1977, pp. 85-100.
- [13] N. Dyn, *Interpolation of scattered data by radial functions*, in *Topics in Multivariate Approximation*, C. K. Chui, L. L. Schumaker, and F. I. Utreras, eds., Academic Press, New York, 1987, pp. 47-61.
- [14] N. Dyn, *Interpolation and approximation by radial and related functions*, in *Approximation theory VI: Volume 1*, C. K. Chui, L. L. Schumaker, and J. D. Ward, eds., Academic Press, New York, pp. 211-234, 1989.
- [15] N. Dyn, D. Levin and S. Rippa, *Numerical procedures for surface fitting of scattered data by radial functions*, *SIAM J. Sci. Statist. Comput.* 7 (1986), pp. 639-659.
- [16] R. Franke, *Scattered Data Interpolation: Tests of Some Methods*, *Math. Comp.* 38 (1982), pp. 181-200.
- [17] R. Franke and G.M. Nelson, *Scattered Data Interpolation of Large Sets of Scattered Data*, *Intl. J. Numerical Methods in Eng.* 15 (1980), pp. 1691-1704.
- [18] R. Franke and G.M. Nelson, *Scattered Data Interpolation and Applications: A Tutorial and Survey*, in *Geometric Modelling: Methods and Their Application*, Berlin: Springer-Verlag, 1991, pp. 131-160.
- [19] W.J. Gordon and J. Wixom, *On Shepard's Method of Metric Interpolation to Scattered Bivariate and Multivariate Data Interpolation*, *Math. Comp.* 32 (1978), pp. 253-264.
- [20] C. A. Glasbey and K. V. Mardia, *A review of image-warping methods*, *Journal of Applied Statistics* 25 (1988), pp. 155-172.
- [21] A. Goshtasby, *Piecewise Cubic Mapping Functions for Image Registration*, *Pattern Recognition* 20 (1987), pp. 525-533.
- [22] R. L. Harder and R. N. Desmarais, *Interpolation using surface splines*, *Journ. Aircraft* 9 (1972), pp. 189-191.
- [23] R.L. Hardy, *Multiquadric Equations of Topography and Other Irregular Surfaces*, *Journal of Geophysical Research* 76 (1971), pp. 1905-1915.
- [24] R.L. Hardy, *Theory and applications of the multiquadric-biharmonic method*, *Comp. Math. Applic.* 19 (1990), pp. 163-208.
- [25] J.T. Kent and K. V. Mardia, *The Link Between Kriging and Thin-plate Splines*, in *Probability, Statistics and Optimization*, F.P. Kelly eds., New York, Wiley, 1994, pp 325-339.
- [26] C.L. Lawson, *Software for C^1 Surface Interpolation*, in *Mathematical Software III*, J.R. Rice, eds., Academic Press, London, 1977, pp. 161-194.
- [27] D. Levin, *The approximation power of moving least-squares*, *Math. Comput.* 67 (1998), pp. 1517-1531.
- [28] D. Levin, *Mesh-independent surface interpolation*, in *Geometric Modeling for Scientific Visualization*, G. Brunnett, B. Hamann, H. Müller and L. Linsen, eds., Springer-Verlag, 2003, pp. 37-49.
- [29] S.K. Lodha and R. Franke, *Scattered Data Techniques for Surfaces*, in *Proceedings of Dagstuhl Conference on Scientific Visualization*, H. Hagen, G. Nielson, and F. Post, eds., IEEE Computer Society Press, 1999, pp. 182-222.
- [30] S. Mann, C. Loop, M. Lounsbery, D. Meyers, J. Painter, T. DeRose, and K. Sloan, *A Survey of Parametric Scattered Data Fitting Using Triangular Interpolations*, in *Curve and Surface Design*, H. Hagen, eds., SIAM, 1992, pp. 145-172.
- [31] J. Manson and S. Schaefer, *Moving least squares coordinates*, *Computer Graphics Forum* 29 (2010), pp. 1517-1524.
- [32] G.M. Nielson and R. Franke, *Surface Construction Based upon Triangulation, Surfaces in CAGD*, R.E. Barnhill and W. Boehm, North-Holland, eds., 1982,

1 pp. 163-179.
 2 [33] P. Percell, "On Cubic and Quartic Clough-Tocher Finite Elements," *SIAM J.*
 3 *Numerical Analysis*, vol. 31, pp. 100-103, 1976.
 4 [34] M.J.D. Powell and M.A. Sabin, *Piecewise Quadratic Approximations on Tri-*
 5 *angles*, ACM Trans. Math. Software 3 (1977), pp. 316-325.
 6 [35] D. Ruprecht and H. Müller, *Free Form Deformation with Scattered Data In-*
 7 *terpolation methods*, Geometric Modelling (Computing Suppl. 8) (1993), pp.
 8 267-281.
 9 [36] D. Ruprecht and H. Müller, *Image Warping with Scattered Data Intepolation*,
 10 IEEE Computer Graphics and Application 15 (1995), pp. 37-43.
 11 [37] R.L. Renka, *Quadratic Shepard Method for Bivariate Interpolation of Scattered*
 12 *Data*, ACM Trans. Math. Software 14 (1988), pp. 149-150.
 13 [38] L.L. Schumaker, *Triangulation Methods*, in *Topics in Multivariate Approxi-*
 14 *mation*, C.K. Chui, L.L. Schumaker, and F. Utreras, eds., Academic Press,
 15 New York, 1987, pp. 219-232.
 16 [39] D. Shepard, *A Two Dimensional Interpolation Function for Irregularly Spaced*
 17 *Data*, Proc. 23rd Nat. Cof. ACM (1968), pp 517-524.
 18 [40] H. Wendland, *Scattered Data Approximation*, Cambridge Monographs on Ap-
 19 *plied and Computational Mathematics*, Cambridge University Press, 2005.
 20 [41] G. Wolberg, *Digital Image Warping*, IEEE Computer Society Press, Los
 21 *Alamitos, CA*, 1994
 22 [42] G. Wolberg, *Image Morphing: A Survey*, The Visual Computer 14 (1998), pp.
 23 360-372.
 24
 25
 26
 27
 28
 29

30 **Appendix**

31 **Singularity in L**

32 Consider the radial basis function $g(r) = r^2$, and examine the $(n+3) \times (n+3)$ matrix
 33 L (equation (2)), when given n distinct points $\{(x_i, y_i)\}_{i=1, \dots, n}$ in \mathbf{R}^2 . Designate
 34 the (i, j) element of L with m_{ij} , $1 \leq i, j \leq n + 3$. Then

$$m_{ij} = \begin{cases} (x_i - x_j)^2 + (y_i - y_j)^2, & \text{if } 1 \leq i, j \leq n, \\ 1, & \text{if } 1 \leq i \leq n, j = n + 1 \\ 1, & \text{if } 1 \leq j \leq n, i = n + 1 \\ x_i, & \text{if } 1 \leq i \leq n, j = n + 2 \\ x_i, & \text{if } 1 \leq j \leq n, i = n + 2 \\ y_i, & \text{if } 1 \leq i \leq n, j = n + 3 \\ y_i, & \text{if } 1 \leq j \leq n, i = n + 3 \\ 0 & \text{otherwise} \end{cases}$$

35 We will show that $rank(L) \leq 6$.

36 It suffices to establish the claim for $n \geq 4$, since the rank of a matrix with size
 37 $(n + 3) \times (n + 3)$ is at most $n + 3$. For $1 \leq i, j \leq n$,

$$m_{ij} = (x_i - x_j)^2 + (y_i - y_j)^2 = (x_i^2 + y_i^2) - 2x_i x_j - 2y_i y_j + (x_j^2 + y_j^2). \tag{5}$$

38 Considering $j=1,2,3$ and k such that $4 \leq k \leq n$, our goal is to find α, β and γ ,
 39 such that $\alpha m_{i1} + \beta m_{i2} + \gamma m_{i3} + m_{ik}$ does not depend on i . From (5), we need the

1 following:

$$2 \quad \alpha + \beta + \gamma + 1 = 0 \quad (6)$$

$$3 \quad \alpha x_1 + \beta x_2 + \gamma x_3 + x_k = 0 \quad (7)$$

$$4 \quad \alpha y_1 + \beta y_2 + \gamma y_3 + y_k = 0. \quad (8)$$

5 We claim that there exists at least one solution to these equations. In fact, if

$$6 \quad \det \begin{bmatrix} 1 & 1 & 1 \\ x_1 & x_2 & x_3 \\ y_1 & y_2 & y_3 \end{bmatrix} \neq 0,$$

7 then there exists exactly one solution. The determinant above is 0 if and only if
 8 (x_1, y_1) , (x_2, y_2) and (x_3, y_3) lay exactly along the same straight line. If all n points
 9 are not on the same straight line, we can change the indices so that the first three
 10 do not form a straight line, in which case the determinant is nonzero. If all n
 11 points are on the same straight line, then $ax_i + by_i + c = 0$ for some a, b and c .
 12 At least one of a or b is nonzero. Without loss of generosity, assume $a \neq 0$. Since
 13 $x_i = -(by_i + c)/a$, (7) can be derived from (6) and (8). Since the points are distinct
 14 and on the same straight line, and $a \neq 0$, y_1, y_2 and y_3 are distinct. Therefore, (6)
 15 and (8) do not conflict and there exist solutions to (6) (7) and (8).

16 Let $\alpha_k, \beta_k, \gamma_k$ be one solution of the joint equations (6) (7) and (8). Then for all
 17 $1 \leq i \leq n$,

$$18 \quad \begin{aligned} & \alpha_k m_{i1} + \beta_k m_{i2} + \gamma_k m_{i3} + m_{ik} \\ & = \alpha_k (x_1^2 + y_1^2) + \beta_k (x_2^2 + y_2^2) + \gamma_k (x_3^2 + y_3^2) + (x_k^2 + y_k^2), \end{aligned}$$

19 which is independent of i . For $n + 1 \leq i \leq n + 3$,

$$20 \quad \alpha_k m_{i1} + \beta_k m_{i2} + \gamma_k m_{i3} + m_{ik} = 0.$$

21 Define

$$22 \quad \delta_k = \alpha_k (x_1^2 + y_1^2) + \beta_k (x_2^2 + y_2^2) + \gamma_k (x_3^2 + y_3^2) + (x_k^2 + y_k^2),$$

23 Then

$$24 \quad \alpha_k m_{i1} + \beta_k m_{i2} + \gamma_k m_{i3} + m_{ik} - \delta_k m_{i,n+1} = 0 \quad \forall i$$

25 which implies that the k 'th column is a linear combination of the first, the second,
 26 the third and the $(n + 1)$ 'st columns. Since this is true for all $4 \leq k \leq n$, the rank
 27 of M is at most 6.

Table

Table 1. Movement of the four background corners following displacement of the tip of the fifth finger by (-15,9); see Figure 15. The last two rows give the sum and the maximum, respectively, of the four distances.

	TPS	r	$r \log r$
Upper-left	(4.5,-2.7)	(4.9,-2.9)	(4.8,-2.9)
Upper-right	(-13.1,7.8)	(-9.7,5.8)	(-10.5,6.3)
Lower-left	(4.4,-2.7)	(7.7,-4.6)	(7.4,-4.5)
Lower-right	(-8.9,5.3)	(-5.2,3.1)	(-5.7,3.4)
Total	36.02	32.02	33.15
Maximum	15.25	11.30	12.25

Figures

Figure 1 - Warping by TPS on Example 1

(a) Original image. (b) Image warped by TPS with A, B, D, E, F, G, and H fixed, and C displaced upward.

Figure 2 - Warping by TPS on Example 2

(a) Original flat surface and 25 control points. (b) Height at the center control point was set to one, and height at each of the other twenty-four control points was set to zero. Intensities off of the control points represent the TPS interpolation. (c) Three-dimensional view of the TPS surface. (d) Intersection of the TPS surface with $y = 0$.

Figure 3 - Warping by Multiquadric on Example 2

Intersection of $y = 0$ with the interpolating multiquadric surface, using parameters: (a) $k = 0$; (b) $k = 6.52$; (c) $k = 30$; (d) $k = 100$.

Figure 4 - Warping by Multiquadric on Example 1

Image warping applied to Figure 1(a), using the radial basis function $g(r) = \sqrt{r^2 + k}$ with (a) $k=0$, and (b) $k = 0.815m$.

Figure 5 - Warping by Inverse Multiquadric on Example 2

Intersection of $y = 0$ with the interpolating inverse multiquadric surface, using parameters: (a) $k = 0$; (b) $k = 10$; (c) $k = 100$; (d) $k = 1000$.

Figure 6 - Warping by Inverse Multiquadric on Example 1

Image warping applied to Figure 1(a), using the radial basis function $g(r) = \frac{1}{\sqrt{r^2+100}}$.

1
2
3
4
5
6
7
8
9
10
11
12
13
14
15
16
17
18
19
20
21
22
23
24
25
26
27
28
29
30
31
32
33
34
35
36
37
38
39
40
41
42
43
44
45
46
47
48
49
50
51
52
53
54
55
56
57
58
59
60

Figure 7 - Warping by Shifted TPS on Example 2

Intersection of $y = 0$ with the interpolating shifted TPS surface, using parameters: (a) $k = 0$; (b) $k = 1$; (c) $k = 10$; (d) $k = 100$.

Figure 8 - Warping by r^k on Example 2

Intersection of $y = 0$ with the interpolating radial basis function surface (r^k), using: (a) $k = 0.5$; (b) $k = 1.5$; (c) $k = 2.5$; (d) $k = 3$.

Figure 9 - Warping by r^k on Example 1

Image warping applied to Figure 1(a), using the radial basis functions (a) $g(r) = r^{0.5}$ (position C highlighted for visibility), and (b) $g(r) = r^{1.5}$.

Figure 10 - Warping by $r \log r$ on Example 2

Intersection of $y = 0$ with the interpolating radial basis function surface ($g(r) = r \log r$).

Figure 11 - Warping by $r \log r$ on Example 1

Image warping applied to Figure 1(a), using the radial basis function $g(r) = r \log r$.

Figure 12 - Warping by Gaussian on Example 2

Intersection of $y = 0$ with the interpolating surface derived from the Gaussian basis function (\exp^{-r^2/k^2}), using parameters: (a) $k = 1$; (b) $k = 2$; (c) $k = 3$; (d) $k = 5$.

Figure 13 - Warping by Gaussian on Example 1

Image warping applied to Figure 1(a), using the Gaussian radial basis function $g(r) = e^{-r^2/100}$.

Figure 14 - Hand Warping

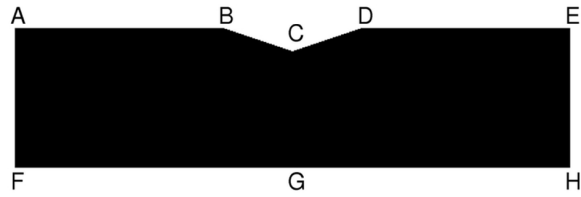
(a) Original image; (b) Control points marked with *.

Figure 15 - Displacement of Fifth Finger

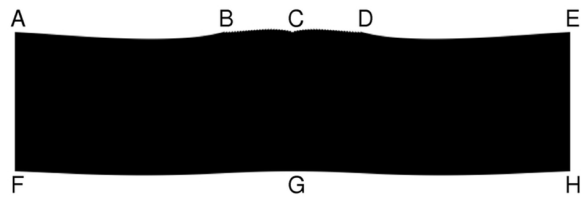
(a) Tip of the smallest finger to be displaced from * to o, with remaining control points fixed; (b) Interpolation with TPS; (c) Interpolation with r ; (d) Interpolation with $r \log r$.

1
2
3
4
5
6
7
8
9
10
11
12
13
14
15
16
17
18
19
20
21
22
23
24
25
26
27
28
29
30
31
32
33
34
35
36
37
38
39
40
41
42
43
44
45
46
47
48
49
50
51
52
53
54
55
56
57
58
59
60

(a) original



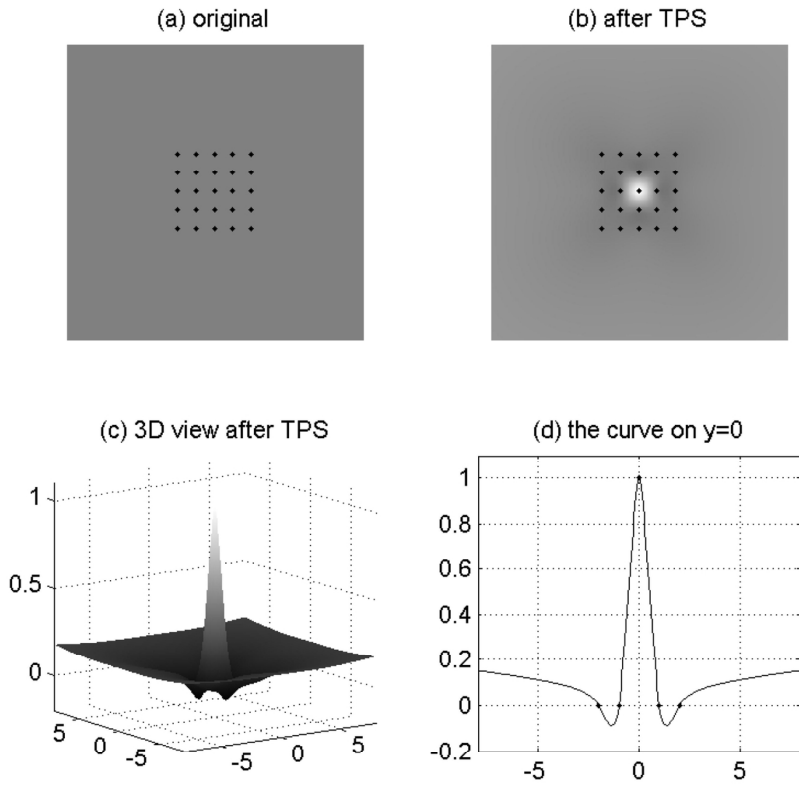
(b) after TPS



107x77mm (300 x 300 DPI)

View Only

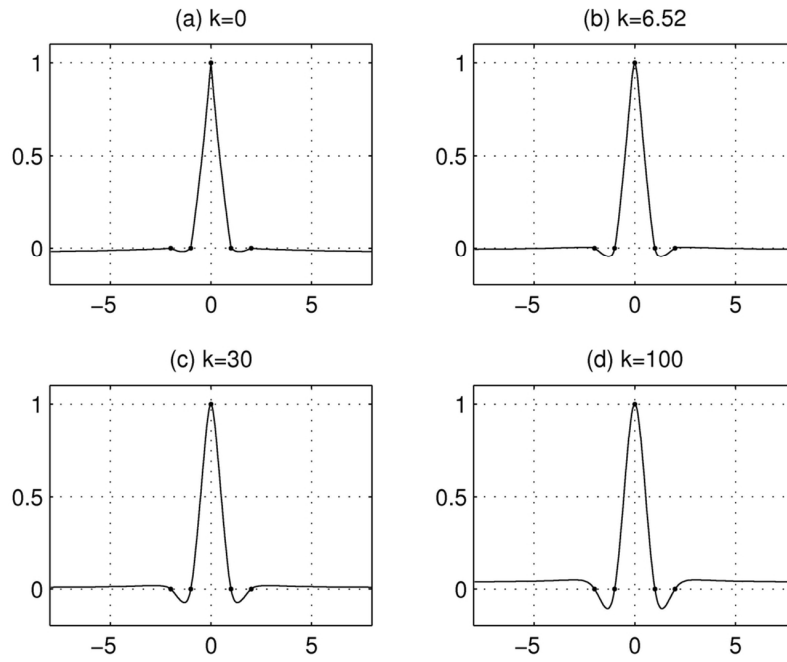
1
2
3
4
5
6
7
8
9
10
11
12
13
14
15
16
17
18
19
20
21
22
23
24
25
26
27
28
29
30
31
32
33
34
35
36
37
38
39
40
41
42
43
44
45
46
47
48
49
50
51
52
53
54
55
56
57
58
59
60



134x121mm (300 x 300 DPI)

Only

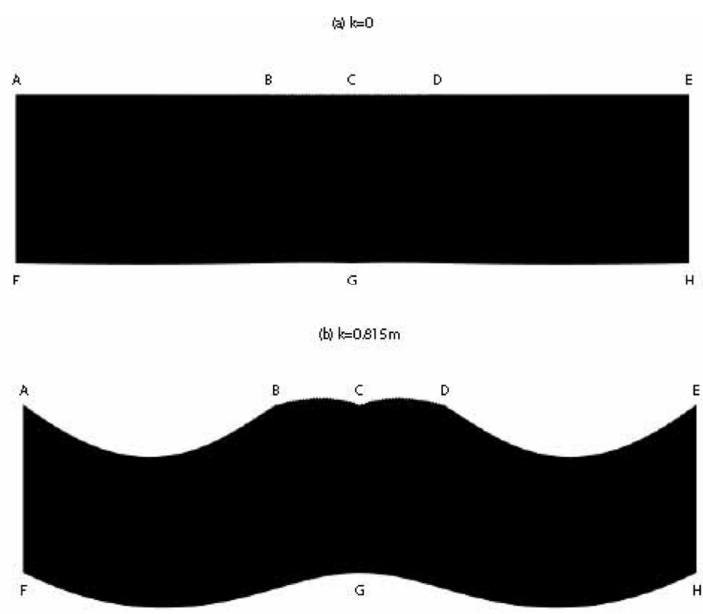
1
2
3
4
5
6
7
8
9
10
11
12
13
14
15
16
17
18
19
20
21
22
23
24
25
26
27
28
29
30
31
32
33
34
35
36
37
38
39
40
41
42
43
44
45
46
47
48
49
50
51
52
53
54
55
56
57
58
59
60



111x83mm (300 x 300 DPI)

View Only

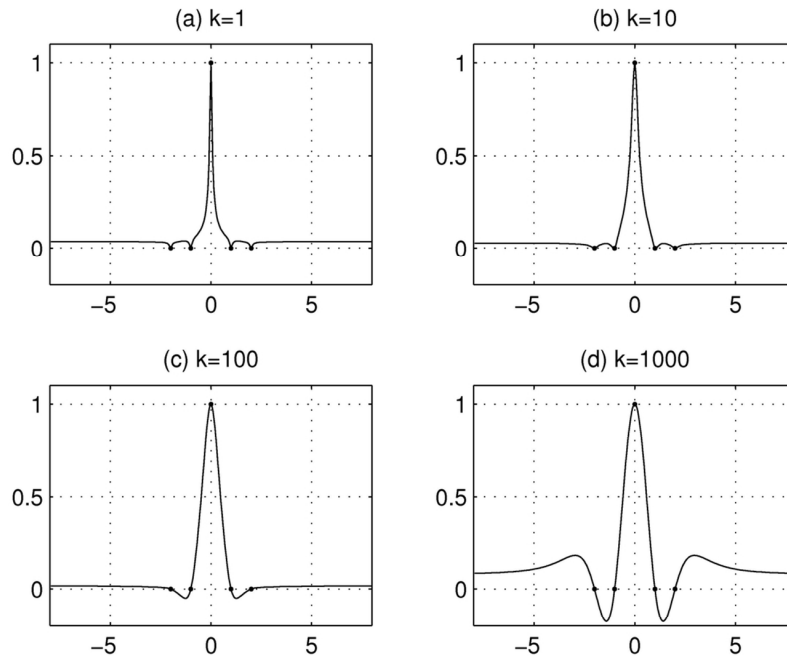
1
2
3
4
5
6
7
8
9
10
11
12
13
14
15
16
17
18
19
20
21
22
23
24
25
26
27
28
29
30
31
32
33
34
35
36
37
38
39
40
41
42
43
44
45
46
47
48
49
50
51
52
53
54
55
56
57
58
59
60



111x72mm (300 x 300 DPI)

Review Only

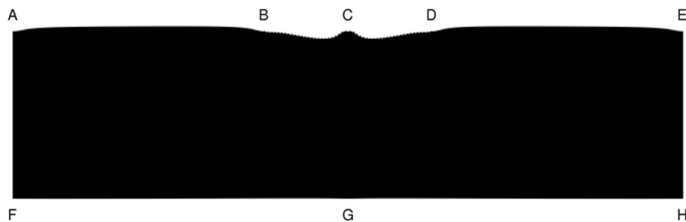
1
2
3
4
5
6
7
8
9
10
11
12
13
14
15
16
17
18
19
20
21
22
23
24
25
26
27
28
29
30
31
32
33
34
35
36
37
38
39
40
41
42
43
44
45
46
47
48
49
50
51
52
53
54
55
56
57
58
59
60



111x83mm (300 x 300 DPI)

iew Only

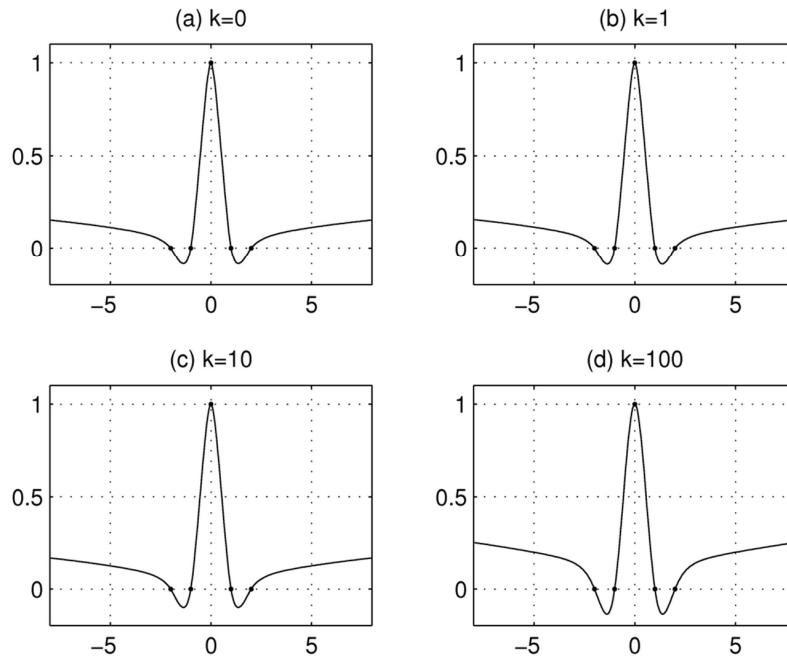
1
2
3
4
5
6
7
8
9
10
11
12
13
14
15
16
17
18
19
20
21
22
23
24
25
26
27
28
29
30
31
32
33
34
35
36
37
38
39
40
41
42
43
44
45
46
47
48
49
50
51
52
53
54
55
56
57
58
59
60



88x34mm (300 x 300 DPI)

Peer Review Only

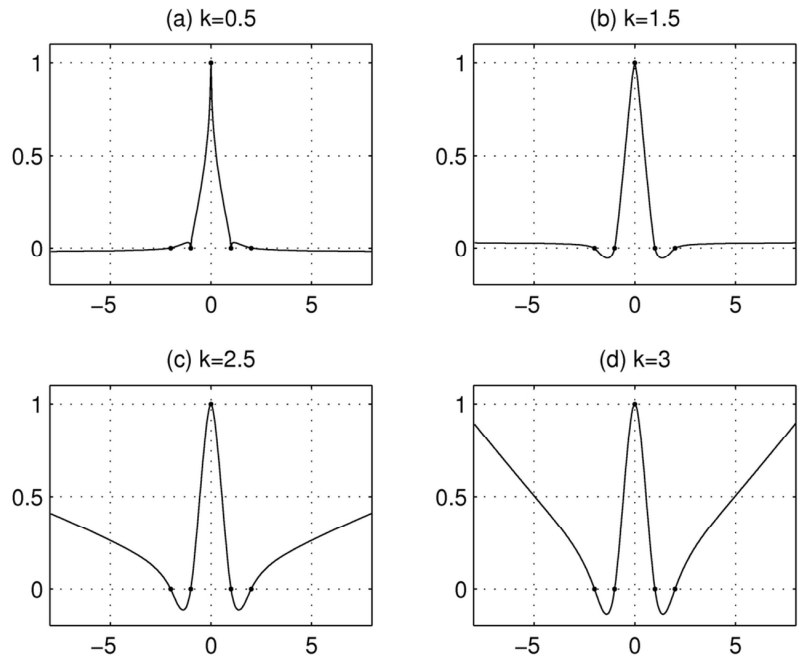
1
2
3
4
5
6
7
8
9
10
11
12
13
14
15
16
17
18
19
20
21
22
23
24
25
26
27
28
29
30
31
32
33
34
35
36
37
38
39
40
41
42
43
44
45
46
47
48
49
50
51
52
53
54
55
56
57
58
59
60



111x83mm (300 x 300 DPI)

View Only

1
2
3
4
5
6
7
8
9
10
11
12
13
14
15
16
17
18
19
20
21
22
23
24
25
26
27
28
29
30
31
32
33
34
35
36
37
38
39
40
41
42
43
44
45
46
47
48
49
50
51
52
53
54
55
56
57
58
59
60

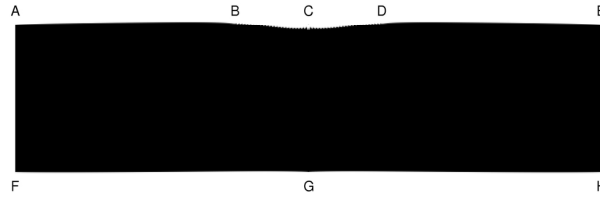


111x83mm (300 x 300 DPI)

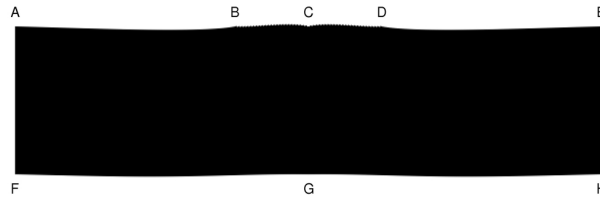
ew Only

1
2
3
4
5
6
7
8
9
10
11
12
13
14
15
16
17
18
19
20
21
22
23
24
25
26
27
28
29
30
31
32
33
34
35
36
37
38
39
40
41
42
43
44
45
46
47
48
49
50
51
52
53
54
55
56
57
58
59
60

(a) $k=0.5$

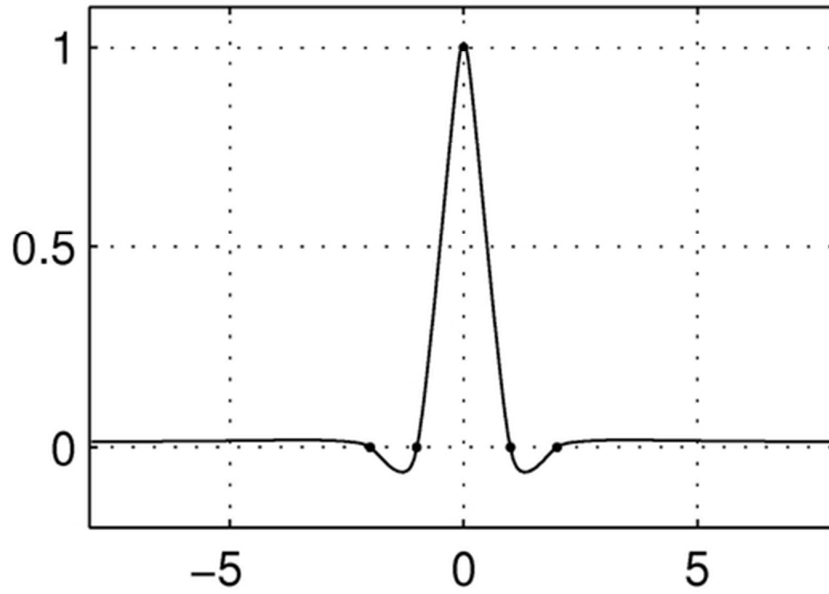


(a) $k=1.5$



182x135mm (300 x 300 DPI)

View Only

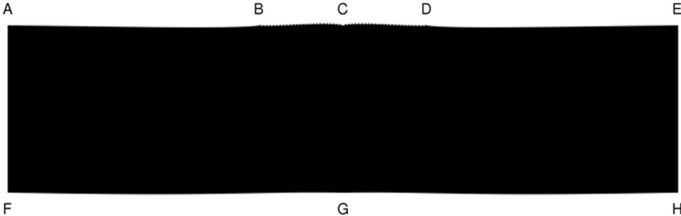


48x32mm (300 x 300 DPI)

Review Only

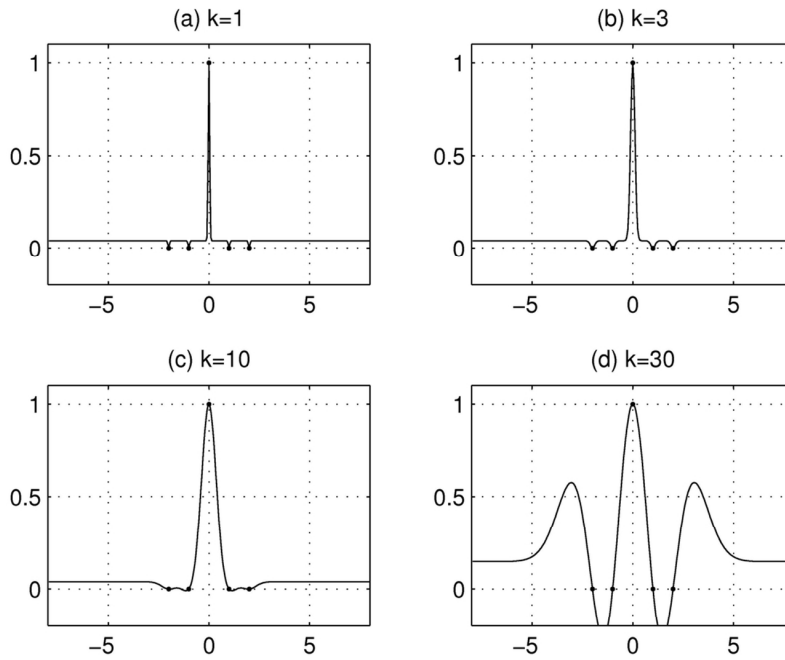
1
2
3
4
5
6
7
8
9
10
11
12
13
14
15
16
17
18
19
20
21
22
23
24
25
26
27
28
29
30
31
32
33
34
35
36
37
38
39
40
41
42
43
44
45
46
47
48
49
50
51
52
53
54
55
56
57
58
59
60

1
2
3
4
5
6
7
8
9
10
11
12
13
14
15
16
17
18
19
20
21
22
23
24
25
26
27
28
29
30
31
32
33
34
35
36
37
38
39
40
41
42
43
44
45
46
47
48
49
50
51
52
53
54
55
56
57
58
59
60



88x34mm (300 x 300 DPI)

Peer Review Only

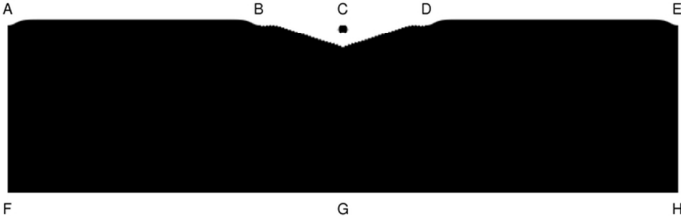


111x83mm (300 x 300 DPI)

ew Only

1
2
3
4
5
6
7
8
9
10
11
12
13
14
15
16
17
18
19
20
21
22
23
24
25
26
27
28
29
30
31
32
33
34
35
36
37
38
39
40
41
42
43
44
45
46
47
48
49
50
51
52
53
54
55
56
57
58
59
60

1
2
3
4
5
6
7
8
9
10
11
12
13
14
15
16
17
18
19
20
21
22
23
24
25
26
27
28
29
30
31
32
33
34
35
36
37
38
39
40
41
42
43
44
45
46
47
48
49
50
51
52
53
54
55
56
57
58
59
60

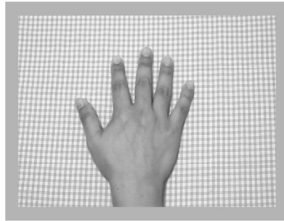


88x34mm (300 x 300 DPI)

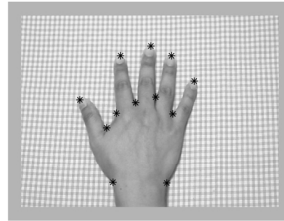
Peer Review Only

1
2
3
4
5
6
7
8
9
10
11
12
13
14
15
16
17
18
19
20
21
22
23
24
25
26
27
28
29
30
31
32
33
34
35
36
37
38
39
40
41
42
43
44
45
46
47
48
49
50
51
52
53
54
55
56
57
58
59
60

(a) original image



(b) reference points and tracking points

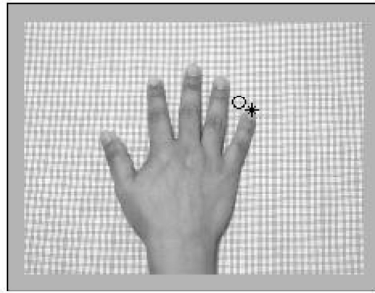


140x69mm (300 x 300 DPI)

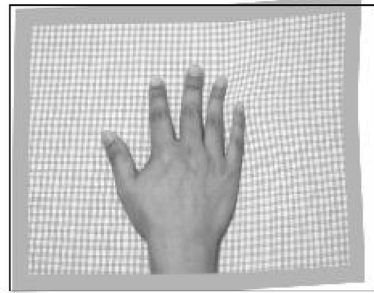
Review Only

1
2
3
4
5
6
7
8
9
10
11
12
13
14
15
16
17
18
19
20
21
22
23
24
25
26
27
28
29
30
31
32
33
34
35
36
37
38
39
40
41
42
43
44
45
46
47
48
49
50
51
52
53
54
55
56
57
58
59
60

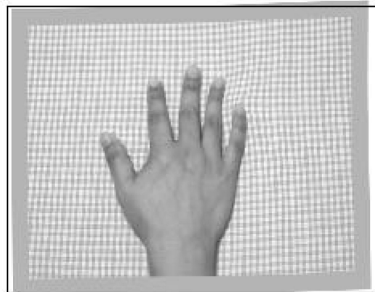
(a) original



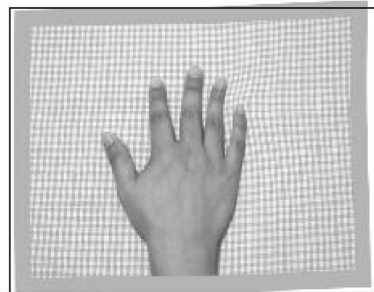
(b) after TPS



(c) after $g(r)=r$



(d) after $g(r)=r \cdot \log(r)$



192x175mm (300 x 300 DPI)

Only